Radio Science, Volume 33, Number 6, Pages 1655–1668, November–December 1998

Model of red sprites due to intracloud fractal lightning discharges

J. A. Valdivia
NRC NASA Goddard Space Flight Center, Greenbelt, MD

G. M. Milikh
Department of Astronomy, University of Maryland, College Park

K. Papadopoulos
Departments of Physics and Astronomy, University of Maryland, College Park

Abstract. A new and improved model of red sprites is presented. Emphasis is placed on accounting for the puzzling observation of the spatial structure in the emissions. The model relies on the electromagnetic pulse (EMP) fields created by a horizontal lightning discharge and includes the observed fractal structure of such discharges in the computation of the EMP power density. It is shown that the model can account for the observed spatial structure of the red sprites while reducing the typical charge required to approximately 100 C.

1. Introduction

High-altitude optical flashes were detected more than 100 years ago [*Kerr*, 1994]. Interest in the subject was renewed recently following the observations of such flashes by the University of Minnesota group [*Franz et al.*, 1990]. Since then, observations of the optical emissions at altitudes between 50 and 90 km associated with thunderstorms have been the focus of many ground and aircraft campaigns [*Boeck et al.*, 1992; *Vaughan et al.*, 1992; *Winckler et al.*, 1993; *Sentman et al.*, 1995; *Lyons*, 1994]. *Sentman and Wescott* [1993] and *Winckler et al.* [1996] described the phenomenon, called "red sprites", as a luminous column that stretches between 50 and 90 km, with peak luminosity in the vicinity of 70-80 km. The flashes have an average lifetime of a few milliseconds and an optical intensity of about 100 kR. Red sprites are associated with the presence of massive thunderstorm clouds, although the luminous columns do not seem to touch the cloud tops. Among the most puzzling aspects of the observations is the presence of spatial structure in the emissions reported by *Winckler et al.* [1996]. Vertical striations with horizontal size of 1 km or smaller, often limited by the instrumental resolution, are apparent in the red sprite emissions.

The first published theoretical model of red sprites [*Milikh et al.*, 1995] associated their generation with transient electric fields induced by large intracloud lightning discharges. The intracloud discharge was modeled as a horizontal electric dipole at an altitude of 10 km, and the field calculation included quasi-static, intermediate, and far-field components. *Milikh et al.* [1995] demonstrated that energization of the ionospheric electrons by the transient fields could account for several of the observed features. Two subsequent papers reached the same conclusions using similar methodology as above but emphasizing different sources for the lightning-generated electric fields. The first [*Pasko et al.*, 1995] modeled the electric fields energizing the electrons as due to a point charge Q (monopole) at an altitude of 10 km. The analysis emphasized the importance of dielectric relaxation of the field. The second [*Rowland et al.*, 1995] assumed that the fields were due to the far

Paper number 98RS02201.
0048-6604/98/98RS-02201$11.00

field of a vertical electric dipole generated by cloud-to-ground discharges. All of the above models, while successful in explaining some observed characteristics of red sprites, such as the color and the generation altitude of the emissions, suffer from two important drawbacks. First, dipole or monopole distributions generate electric fields smoothly distributed at ionospheric heights, thereby failing to account for the persistent spatial structure of the red sprites. Second, the threshold charge and dipole moment requirements for all three models have been criticized as unrealistically large (based on the lightning parameters cited by *Uman* [1987]).

The objective of the present paper is to extend the results of *Milikh et al.* [1995] and it Valdivia et al. [1997] by incorporating in the calculation of the transient field the internal fine structure of the intracloud discharge. It will be shown that incorporating in the calculation of the lightning-induced fields the dendritic fine structure of the lightning channel, as described by *Williams* [1988] and by *Lyons* [1994] (who termed it spider lightning), results in a natural explanation of the observed spatial structure of the red sprites and in a significant reduction of the required threshold charge. The fractal lightning discharge must be of the intracloud type to have a radiation pattern that is preferentially upward (as well as downward).

Figure 1 illustrates the major elements used in our model. The first element is a computer model of the intracloud discharge that tries to account for its dendritic fine structure. This is modeled as a horizontal fractal discharge structure that produces the spatiotemporal distribution of the amplitude and phase of the electromagnetic field in the far zone.

As the field propagates from the lower atmosphere, self-absorption becomes important, requiring, as the next element of our model, the self-consistent computation of the propagation of the lightning-induced fields in the lower ionosphere. The fields interact with and energize the ambient electrons generating non-Maxwellian distribution functions. The collisions of energetic electrons with neutral particles result in the observed emissions. The structuring of the emissions is attributed to the highly inhomogeneous fields projected into the lower ionosphere, when the internal structure of the discharge is included in the model. It will be shown that the model not only accounts for the structure but also simultaneously reduces the required charge for the lightning discharge

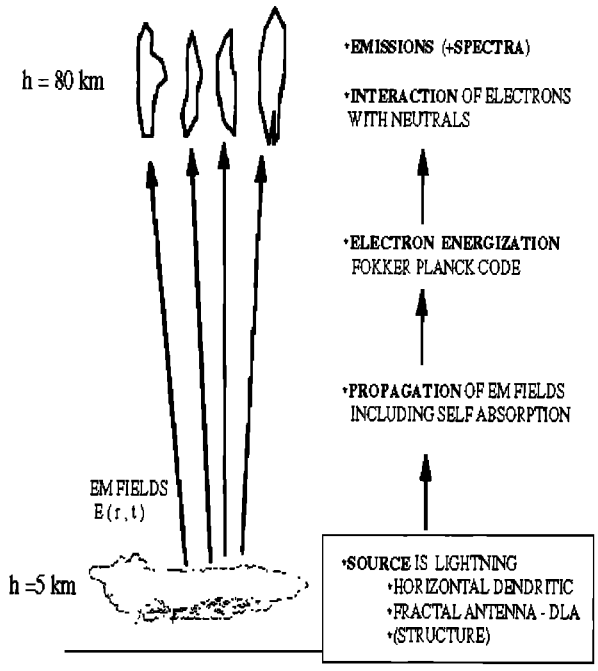

Figure 1. A diagram of the tasks involved in the treatment. From the fractal structure, we compute the fields generated and their interaction with the medium in the lower ionosphere.

driving the red sprites, which have a total optical emission of about 100 kR, to levels more consistent with observational requirements.

In section 2 we describe a model of lightning as a fractal antenna, estimate its fractal dimension, and present a few examples of fractal discharges. In section 3 we consider the propagation of the lightning-generated fields in the lower ionosphere, including the effect of self-absorption, and compute the electron distribution function in the presence of the electric fields. In section 4 we discuss the intensity of the optical emissions due to lightning and the spatial structure of the red sprites generated by fractal discharges. This is followed in section 5 by conclusions.

2. Lightning as a Fractal Antenna

It is well known that lightning discharges follow a tortuous path [*Le Vine and Meneghini*, 1978]. It was shown [*Williams*, 1988] that intracloud discharges resemble the well-known Lichtenberg patterns observed in dielectric breakdown [see also *Idone*, 1995].

These patterns have been recently identified as fractal structures of the diffusion limited aggregate (DLA) type with a fractal dimension $D \approx 1.6$ [*Niemeyer et al.*, 1984; *Sander*, 1986].

A fractal lightning discharge radiates as a fractal antenna and, unlike a dipole type of antenna, generates a spatially nonuniform radiation pattern, with regions of high field intensity and regions of low field intensity. This is equivalent to a two-dimensional phased array having an effective gain factor. Such a fractal lightning discharge can be modeled as a set of nonuniform distributed small current line elements [*Niemeyer et al.*, 1984; *Vecchi et al.*, 1994] $\{\mathbf{r_n}, \mathbf{L_n}, \mathbf{I_n}, \mathbf{s_n}) | \mathbf{n} = \mathbf{0}, ..., \mathbf{N}\}$, where $\mathbf{r_n}$ and $\mathbf{L_n}$ are the position and orientation of the nth line element, s_n is the distance traveled by the discharge, and I_n is the strength of the current at the nth line element. For future reference, the discharge is placed horizontally at a height of 5 km, and an image discharge is placed 5 km below the conductive ground.

2.1. Why Is a Fractal Lightning Discharge so relevant?

A fractal lightning discharge can be considered as a two-dimensional phased array antenna that will naturally exhibit a spatially dependent radiation pattern with an effective gain factor. Such a gain factor is extremely important, for it will reduce the lightning energetics (see below), compared with the dipole model, required to produced the optical emissions in the ionosphere.

In order to study how this gain factor comes about, we consider a fractal antenna as a nonuniform distribution of radiating elements as described above. For an oscillating current of the form $e^{i\omega t}$, each of the elements contributes to the total radiated power density at a given point with a vectorial amplitude and phase [*Allain and Cloitre*, 1987; *Jaggard*, 1990; *Werner and Werner*, 1995], i.e.,

$$\mathbf{E} \cdot \mathbf{E}^* \sim \left(\sum_{\mathbf{n=1}}^{\mathbf{N}} \mathbf{A_n} e^{\mathbf{i}\phi_n}\right) \cdot \left(\sum_{\mathbf{m=1}}^{\mathbf{N}} \mathbf{A_m} e^{\mathbf{i}\phi_m}\right)^*$$

$$= \sum_{n,m} (\mathbf{A_n} \cdot \mathbf{A_m^*}) e^{\mathbf{i}(\phi_n - \phi_m)} \qquad (1)$$

where $\mathbf{E}^*$ denotes the complex conjugate. The vector amplitudes $\mathbf{A}_n$ represent the strength and orientation of the field generated by each of the individual elements, while the phases ϕ_n are, in general, related to the spatial distribution of the individual elements over the fractal. In fact, for an oscillating current of the form $e^{i\omega t}$ the phases vary as $\phi \approx \mathbf{k} \cdot \mathbf{x} - \mathbf{k} \cdot \mathbf{r_n}$, where $k = \omega/c$ and $\mathbf{x}$ is the position of the observation point.

In the sense of statistical optics, we can consider the ensemble average of equation (1), using an ergodic principle, over the spatial distribution $P(\phi_1, \phi_2, \phi_3, ..., \mathbf{A_1}, \mathbf{A_2}, \mathbf{A_3}, ...)$ of the fractal elements [*Goodman*, 1985]. For simplicity we assume that the distributions for each of the elements are independent and the same; hence

$$G \equiv \sum_{n,m}^{N} \left\langle (\mathbf{A_n} \cdot \mathbf{A_m^*}) e^{\mathbf{i}(\phi_n - \phi_m)} \right\rangle$$

From this equation the antenna gain G yields

$$G = N^2 \left(\frac{\left\langle |\mathbf{A}|^2 \right\rangle}{N} + \frac{N-1}{N} |\langle \mathbf{A} \rangle|^2 \left| \left\langle e^{i\phi} \right\rangle \right|^2 \right)$$

This is one of the most important relationships that can be used to study fractal antennae. The first term represents the incoherent radiation component, and the second term is the coherent (interference) radiation component. If we further assume that $\left\langle |\mathbf{A}|^2 \right\rangle = |\langle \mathbf{A} \rangle|^2 = 1$, we obtain that the ensemble average is

$$\langle \mathbf{E} \cdot \mathbf{E}^* \rangle \sim G = N^2 \left(\frac{1}{N} + \frac{N-1}{N} \left| \left\langle e^{i\phi} \right\rangle \right|^2 \right) \qquad (2)$$

If the distribution of the phases is random (or uniform), then $< e^{i\phi} >= 0$ and $G = N$. On the other hand, if there is perfect coherence, we have $< e^{i\phi} >= 1$ and $G = N^2$. If the distribution of the vector amplitudes does not satisfy the above relations, for example, if the radiators are oriented in arbitrary directions, then the power density will be less coherent since $\left\langle |\mathbf{A}|^2 \right\rangle \geq |\langle \mathbf{A} \rangle|^2$ (true for any distribution). A similar result can be achieved by having a distribution of amplitudes instead of phases.

In general, a fractal antenna will display partial coherence in some direction(s), and the peak radiated power will lie in between these two limits and can show a significant gain over a random distribution of phases. The coherence term $N(N-1) |\langle \mathbf{A} \rangle|^2 \left| \left\langle e^{i\phi} \right\rangle \right|^2$ depends on the spatial structure of the fractal antenna. Such spatial structure is usually described by the fractal dimension D [*Ott*, 1993]. We conjecture

that the most relevant structural parameter determining the radiation pattern of a fractal discharge is its fractal dimension, which we can estimate as follows. If we partition the volume where the discharge occurs into boxes of side ε, the number of boxes that contain at least one of the discharge elements will scale as $N(\varepsilon) \sim \varepsilon^{-D}$. It is easy to verify that a point corresponds to $D = 0$, a line corresponds to $D = 1$, and a compact surface corresponds to $D = 2$. The box counting dimension [*Ott*, 1993] is then defined by

$$D \simeq \frac{\ln N(\varepsilon)}{\ln(\frac{1}{\varepsilon})} \tag{3}$$

Note that if ε is too small, then the elements of the discharge will look like one-dimensional line elements. Similarly, if ε is too large, then the discharge will appear as a single point. Therefore it is very important to compute D only in the scaling range, which is hopefully over a few decades in ε.

We will now apply these ideas to models of the lightning discharge. Figure 2 shows two different models of a lightning discharge. The top drawing shows the dipole, or linear, model of the current channel between two points; in general, it will generate a dipole radiation pattern. The middle drawing shows a tortuous model of the discharge between the same two points; this tortuous current channel can be considered as a two-dimensional phased array, as shown in the bottom drawing. Note that the tortuous model will have a longer path length that will increase N or the individual A_n in equation (2) with respect to the dipole model. Clearly, there will be positions at which the radiation pattern from the tortuous line elements will add constructively, while at other positions they will add destructively. Therefore we expect that a tortuous lightning channel will have, besides the spatial structure, a radiation pattern with spots of radiated power density larger than the more homogeneous dipole pattern. The fractal dimension will be an important parametrization for the fractal discharge models that will be generated and will play a significant role in the spatial structure and intensity of the radiation pattern, as we will see later.

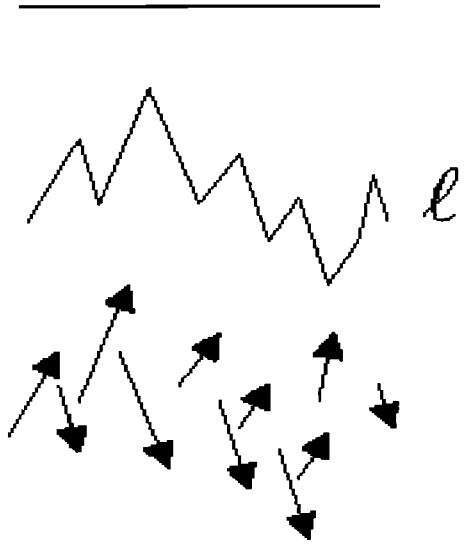

Figure 2. Top drawing is a dipole or straight line model of the lightning discharge. Middle drawing represents the tortuous model between the same two endpoints as in the dipole model. The tortuous model can be described as a spatially nonuniform distribution of radiators, each contributing to the total radiation field with a given phase and amplitude (bottom drawing).

2.2. Time Dependent Fields

A current pulse, $I(t - s/v)$, propagates with speed v (hence $\beta = v/c$), along the length s of the horizontal fractal discharge. The discharge will be mainly horizontal so that it radiates energy upward, as opposed to a vertical discharge, which will radiate its energy mainly in the horizontal direction. The intracloud current pulse is taken as a series of train pulses that propagate along the arms of the antenna and have a time dependence given by

$$I(t) = (e^{-\alpha t} - e^{-\gamma t})(1 + \cos(\omega t))H(t) \tag{4}$$

with $\omega = 2\pi\alpha n_f$ and $H(t)$ as the step function. Here n_f represent the number of oscillations during the decay timescale $1/\alpha$. We chose $\alpha = 10^3$ s^{-1} as the inverse duration of the pulse and $\gamma = 2 \times 10^5$ s^{-1} as the risetime [see *Uman*, 1987]. The initial strengths of the current pulse I_o get divided as the discharge branches, but the total charge discharged is then $Q = I_o/\alpha$, which for $I_o = 100$ kA gives $Q \approx 100$ C.

2.3. Example: Tortuous Discharge Model

A fractal tortuous path can be constructed in terms of a random walk between two endpoints [*Vecchi et al.*, 1994]. We start with a straight line of length L, to which the midpoint is displaced using a Gaussian random generator with zero average and

deviation σ (usually $\sigma = 0.5L$). The procedure is then repeated to each of the straight segments N times. There is a clear repetition in successive halving of the structure as we go to smaller scales, making it a broadband antenna. Figure 3a shows a typical tortuous fractal, where the division has been taken to the $N = 8$ level and in which the path length S has increased 5 times, i.e., $S \approx 5L$. We can estimate the fractal dimension by realizing that the total path length S should go as

$$S \sim L(\frac{L}{\langle \ell \rangle})^{D-1} \tag{5}$$

where $\langle \ell \rangle$ is the average segment size. This equation can be derived from equation (3).

The computation of the radiated electric field is described in the appendix in the far-field approximation. Note that this antenna will radiate every time there is a change in direction of the discharge. It is expected that it will have a peak radiated power density larger than that of an equivalent dipole (see description on antenna gain above).

The far-field array factor $R = \alpha \int dt \mathbf{E^2}$ and the peak power density depend on the path length or, equivalently, on the number of segments of the fractal. Take the tortuous path of Figure 3a with $n_f = 5$ so that the peak of the array factor is at $x = 0$ km and $y = 0$ km at a height $h = 60$ km. Starting with the dipole (straight path), for each successive division, $N = 1, 2, ..., 8$, we compute the array factor R as a function of the tortuous path length (Figure 3b). There is a clear increase in the array factor from the tortuous fractal as compared with the single dipole. The straight line fit agrees with the theoretical result (to be published elsewhere)

$$\frac{R(\Delta s)}{R_o} \approx 1 + \alpha \Delta t \, n_f \, \frac{\Delta s}{L_o}$$

where Δs is the increase in the path length due to the tortuosity and Δt is the time it takes the pulse to propagate along the fractal.

Therefore, even for time dependent discharge currents, the effect of tortuosity can definitely increase the radiated power density at certain locations, as compared with a single dipole antenna. Such a result will become extremely important in our lightning studies, in which by going away from single dipole models we can increase the power radiated from a fractal antenna or, in the case of lightning, a fractal discharge. Such gain in the radiated power density can be traced to the different fractal dimensions D as given by equation (5).

Another important concept related to fractal antennae is the spatial structure of the radiation field.

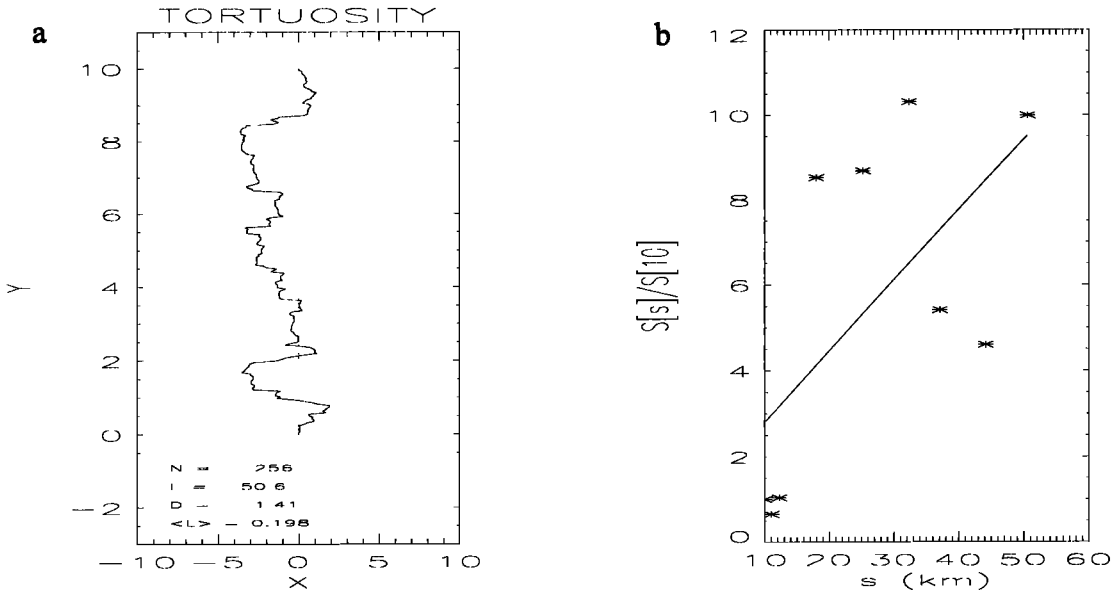

Figure 3. (a) The tortuous discharge. (b) The array factor dependence, normalized to the dipole, on the path length.

For large n_f the array factor scales as $R \sim exp(-\alpha \Delta r/c)(2 + \cos(2\pi\ n_f\ \alpha\Delta r/c))$ where $\Delta r = \max_n d_n = \max_n \parallel \mathbf{x} - \mathbf{r_n} \parallel$, i.e., the maximum variation over the fractal of the distance between the elements of the fractal r_n and the field position $\mathbf{x}$ (see the appendix). Consequently, the radiation pattern will have spatial structure when $\alpha\ n_f\ \Delta r/c > 2\pi$, which translate into $n_f > 50$. A more comprehensive and natural model of fractal discharges that includes branching and tortuosity is developed in the next section.

2.4. Two-Dimensional Fractal Discharge

Femia et al. [1993] found experimentally that a dielectric discharge pattern is approximately an equipotential. On the basis of this idea, we can construct a fractal discharge by adapting for our purposes the two-dimensional stochastic dielectric discharge model proposed by *Niemeyer et al.* [1984]. This model naturally leads to fractal structures where the fractal dimension can be easily parametrized by a parameter η.

We start with a charge Q at the center of our computational box. A discharge will start propagating from this initial point. Consider a discharge pattern (line connecting the solid circles in Figure 4) at a later time t, which we assume to be an equipotential with value $\phi = 0$. The boundary condition at infinity (on a circle far away from the discharge) is $\phi = 1$, a choice that simplifies the computation of the electric field close to the discharge. The potential outside the discharge structure can be computed by iterating the discrete two-dimensional Laplace's equation

$$\nabla^2\phi = 0$$
$$\phi_{i,j} = \tfrac{1}{4}(\phi_{i+1,j} + \phi_{i-1,j} + \phi_{i,j+1} + \phi_{i,j-1})$$

until it converges. The discharge pattern grows in single steps by the addition of an adjacent grid point (open circles in Figure 4) to the discharge pattern, generating a new bond. We assume here that an adjacent grid point, denoted *(i,j)*, has a probability proportional to the η power of the local electric field to become part of the pattern. Since the electric field for a point *(i,j)* adjacent to the discharge (where $\phi = 0$) is given by $E_{i,j} \sim \phi_{i,j}$, the probability of adding such a point to the discharge can be expressed as

$$p(i,j) = \frac{\phi_{i,j}^{\eta}}{\sum_{l,m} \phi_{l,m}^{\eta}}$$

where the normalization sum is over all the points adjacent to the discharge. Therefore we apply the Monte Carlo method to add one of the adjacent points to the discharge, i.e., throw the dice and choose one of the adjacent points. The new grid point, being part of the discharge structure, will have the same potential as the discharge pattern, i.e., $\phi = 0$. Therefore we must resolve Laplace's equation for the potential every time we add a new bond.

The structure generated for $\eta = 1$ corresponds to a Lichtenberg pattern. The dimension of this fractal structure is $D \simeq 1.5$, as follows from Figure 5, which reveals the relation between η and D (defined above and computed with the standard methods [*Ott*, 1993]).

We expect that when $\eta = 0$ the discharge will have the same probability of propagating in any direction; the discharge will be a compact structure with a dimension $D = 2$. On the other extreme, for $\eta \to \infty$ the discharge will become one dimensional, and hence $D = 1$. Therefore this model, and also the dimension of the discharge, is parametrized by η (Figure 6).

In order to compute the radiated fields, we must describe the current along each of the segments of the fractal discharge. We start with a charge Q at the center of the discharge. The current is then discharged along each of the dendritic arms. At each

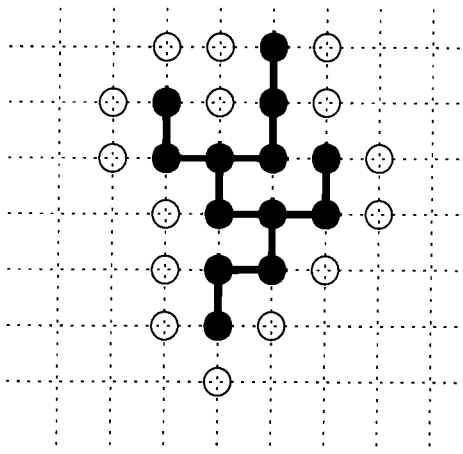

Figure 4. Diagram of the discretized fractal discharge and its adjacent grid points. The solid circles correspond to the discharge, and the open circles correspond to the adjacent points that can be added to the discharge.

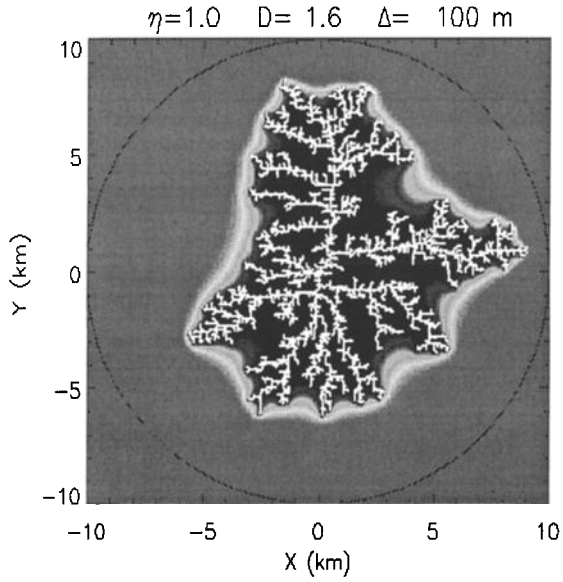

Figure 5. Fractal discharge generated with the stochastic model for $\eta = 1$. The gray shading corresponds to the electric potential that generated the discharge.

branching point we choose to ensure conservation of current, but we expect a high current to propagate longer than a small current before being stopped. Hence at each branching point a larger fraction of the current will propagate along the longest arm. Suppose that a current I_o arrives at a given branching point, and if L_i is the longest distance along the ith branching arm, we assume that the current on the ith arm will be proportional to L_i^η. Therefore we can satisfy charge (or current) conservation if the current along the ith arm, which branches at the branching point, is

$$I_i = \frac{L_i^\eta}{\sum_j L_j^\eta}. \tag{6}$$

The calculation of the electric field in the ionosphere from the fractal current structure is described in the appendix for the far field of the small line elements. It turns out that the radiated power density $S(\mathrm{W/m^2}) = c\epsilon_o E^2 \approx I_o^2 \beta^2 f(D) g(\theta, D, \beta)$, where $g(\theta, D, \beta)$ describes the angular distribution of the radiated pattern and $f(D)$ describes the dimension dependence. As we increase β, the angular field distribution from a single horizontal line element becomes narrower and goes from a dipole radiation pattern that peaks in the direction perpendicular to $\widehat{\mathbf{L}}_n$ (contributes to the field in ionosphere) to a radiation pattern that peaks preferentially in the same direction as $\widehat{\mathbf{L}}_n$ (does not contribute to the field in the ionosphere). Therefore there is also an interplay between the electric field pattern $g(\theta)$ generated from the fractal discharge, and hence between its dimension and speed of propagation β.

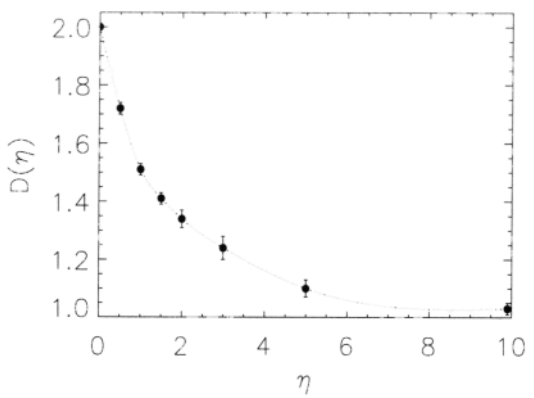

Figure 6. The dimension of the stochastic discharge model as a function of η with the estimated error bars.

3. Electromagnetic Pulse Absorption and Electron Energization

Once we have the fractal discharge structure, we must consider the propagation of the lightning fields indiced in the lower ionosphere. The fields energize the electrons, generating highly non-Maxwellian electron distribution functions which increase the number of electron-neutral inelastic collisions, responsible for the emissions, and inducing field self-absorption. The electron energization is computed with the help of a Fokker-Planck code [*Tsang et al.*, 1991].

3.1. Self-Absorption

As the lightning-induced fields propagate in the lower ionosphere, the field changes the properties of the medium by heating the electrons while experiencing absorption. The solution to Maxwell's equations for the propagation of the electric field is a nonlinear wave equation

$$\nabla^2 \mathbf{E} - \nabla(\nabla \cdot \mathbf{E}) - \frac{4\pi}{c^2} \frac{\partial}{\partial t}(\hat{\sigma}\mathbf{E}) - \frac{1}{c^2} \frac{\partial^2}{\partial t^2}(\hat{\varepsilon}\mathbf{E}) = 0, \tag{7}$$

where the medium is incorporated in the conductivity $\hat{\sigma}$ and in the dielectric $\hat{\varepsilon}$ tensors [*Gurevich*, 1978]. For the heights and frequencies of interest, $\hat{\sigma}$ and $\hat{\varepsilon}$ reach a steady state much faster than the timescale of the field variation, i.e., $1/\omega$. The solution in the ray approximation is therefore

$$E^2(\hat{r}s,t) \simeq \frac{E^2(0,t-\frac{s}{c})}{s^2} H(t-\frac{s}{c}) e^{-\csc(\chi)\int_0^z \kappa(z,E^2)dz}, \quad (8)$$

where $\sin(\chi) = z/\sqrt{x^2+y^2+z^2}$ is the elevation angle of the point $\mathbf{r} = \hat{\mathbf{r}}\mathbf{s} = \{\mathbf{x},\mathbf{y},\mathbf{z}\}$, $H(t)$ is the step function, $\kappa(z,E^2) = \omega_e^2\nu_e/c(\Omega^2+\nu_e^2)$ is the absorption coefficient of the wave, $\omega_e^2 = 4\pi n_e e^2/m$ is the plasma frequency, and $\Omega = eB/mc$ is the electron gyrofrequency. The nonlinearity is incorporated self-consistently through $\nu_e = \nu_e(z,|E|)$, the electron-neutral collision frequency, due to the non-Maxwellian nature of the electron distribution function that the fields generate.

3.2. Electron Distribution and the Fokker-Planck Approach

The electron distribution function in the presence of an electric field is strongly non-Maxwellian, requiring a kinetic treatment. The kinetic treatment will provide $\nu_e = \nu_e(z,|E|)$ and the excitation rates of the different electronic levels. We use an existing Fokker–Planck code, which has been developed for the description of ionospheric RF breakdown [*Tsang et al.*, 1991; *Papadopoulos et al.*, 1993]. For given values of E and ν_o (the ambient collisional frequency), the electron distribution function $f(\mathrm{v})$ is found by solving numerically the Fokker-Planck equation

$$\frac{\partial f}{\partial t} - \frac{1}{3m\mathrm{v}^2}\frac{\partial}{\partial \mathrm{v}}(\mathrm{v}^2\nu(\mathrm{v})\tilde{\epsilon}(E,\nu(\mathrm{v}))\frac{\partial \mathrm{f}}{\partial \mathrm{v}}) = \pounds(f), \quad (9)$$

where

$$\tilde{\epsilon}(E,\nu) = \frac{e^2E_o^2}{m[\Omega_B^2+\nu^2]}\{1+(\frac{\Omega_B}{\nu})^2\cos^2\theta_o\} \quad (10)$$

is the quiver energy or the kinetic electron energy in an oscillating electric field, $\nu(\mathrm{v})$ is the electron-neutral effective collisional frequency, $\pounds$ is the operator which describes the effect of the inelastic collisions [*Tsang et al.*, 1991], and θ_o is the angle between the electric and magnetic fields. We have assumed that the frequency of the electromagnetic fields satisfies $\omega \ll \Omega_B, \nu_e$. We have also assumed that $(\Omega_B/\nu)^2\cos^2\theta_o < 1$, which is the less energetically beneficial case. It is satisfied at any height of the lower ionosphere in the equatorial region or at the height below 80 km at middle latitude. Notice that for $(\Omega_B/\nu)^2\cos^2\theta_o < 1$, the electrons can gain more energy from the electric field, increasing the absorption and reducing the field amplitude at the higher altitudes.

The averaged quiver energy $\tilde{\epsilon}(E,\nu_e)$, which depends nonlinearly on the steady state averaged collisional frequency ν_e, is the critical parameter that controls the behavior of the distribution function $f(\mathrm{v})$ under an electric field E at a given height. For values of $\tilde{\epsilon} < 0.02$ eV, most of the energy absorbed by the electrons excites the low-lying vibrational levels of nitrogen, and emissions in the visible range cannot be excited. For 0.02 eV$< \tilde{\epsilon} < 0.1$, eV the electron energy results in excitation of optical emissions and molecular dissociation. For $\tilde{\epsilon} > 0.1$ eV, ionization is initiated. For simplicity we are going to consider the case in which the electric field is below the ionization threshold, i.e., $\tilde{\epsilon} < 0.1$ eV; otherwise a self-consistent equation for the electron density in space must be included in the analysis.

4. Intensity and Structure of Sprites

Given the spatiotemporal field profile including self-absorption, we consider the optical emissions, or red sprites, from N_2. We discuss only the emissions of the $N_2(1P)$ band caused by the excitation of the $B^3\Pi_g$ electronic level of molecular nitrogen by electron impact. This band dominates in the spectrum of red sprites [*Mende et al.*, 1995]. Here we compute the excitation rate ν_{ex}^B of the $N_2(B^3\Pi_g)$ electronic level, which has an excitation energy of 7.35 eV and a lifetime of 8 μsec, by using the Fokker-Planck code for a given field strength. The excitation rate per electron is then given by

$$\nu_{ex}^B = 4\pi N_{N_2}\int f(\mathrm{v})\mathrm{v}^3\sigma_{ex}^B(\mathrm{v})d\mathrm{v}, \quad (11)$$

where σ_{ex}^B is the excitation cross section and N_{N_2} is the number density of N_2 [*Milikh et al.*, 1997]. The excitations are then followed by optical emissions, and the number of photons emitted per second per cubic centimeter is given by $\nu_{ex}^B n_e$ for an electron density n_e. In order to compare with observations, it is convenient to average in time the number of photons over the duration of the discharge T (approximately milliseconds), i.e., $< \nu_{ex}^B n_e >=$

$\int_0^T \nu_{ex}^B n_e dt/T$. The intensity of the radiative transition in Rayleighs is given by

$$I = \frac{10^{-6}}{4\pi} \int < \nu_{ex}^B n_e > dl, \qquad (12)$$

where the integral is carried along the visual path of the detector (column integrated).

In order to apply our model, we must specify the current amplitude I_o, along the discharge, the velocity of propagation of the discharge β = v/c and the electron density profile in the lower ionosphere. From here on we shall assume a midlatitude nighttime electron density profile [*Gurevich*, 1978].

The fractal model is especially suitable for understanding the dependence on the dimension of the discharge [*Valdivia et al.*, 1997], since $D(\eta)$ can be easily parametrized, as is plotted in Figure 6. We proceed next to determine the spatial structure of the optical emissions as a function of the dimension D. We consider the four fractal discharges $\eta = 1, 2, 3$, and ∞ shown in Figure 7 with dimensions $D \simeq 1.5$, 1.35, 1.25, and 1.0, respectively, where the thickness of the line corresponds to the strength of the current.

In general, the electric field and emission pattern induced by the fractal discharges in the ionosphere are three-dimensional (3-D), but for the purposes of illustration we take a two-dimensional cross section (e.g., the line $y = 10$ km from the center of the discharge) of this 3-D profile in the ionosphere. The emission patterns along the cross section $y = 10$ km, averaged over the duration of the discharge using Equation (12), are shown in Figure 8 for the fractal discharge corresponding to $\eta = 3$. The velocity of the discharge was taken as $\beta = 0.025$ and the amount of current was taken as $I_o = 200$ kA. The emission rate, i.e., number of photons per cubic centimeter per second, is computed in decibels with respect to the averaged emission rate over the image area. The

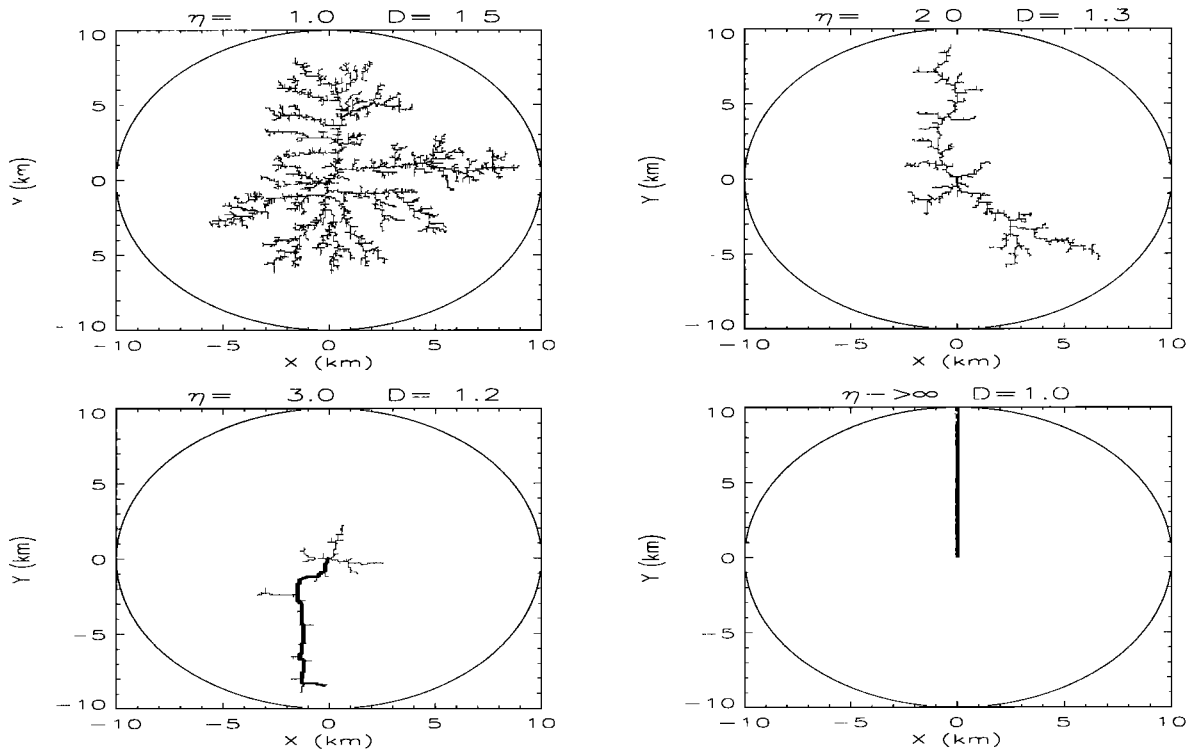

Figure 7. The fractal structures for dimensions D= 1.5, 1.35, 1.25 and 1.0 ($\eta = 1, 2, 3$, and ∞). The thickness of the lines corresponds to the current strength, and current conservation has been satisfied at each branching point.

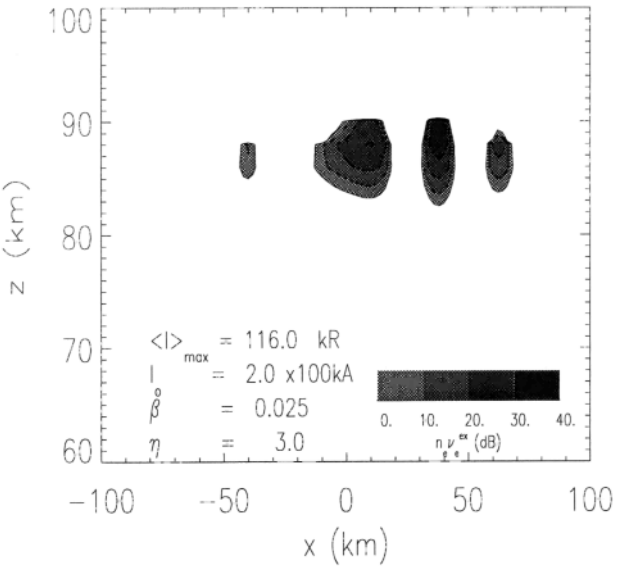

Figure 8. The time-averaged emission pattern for $\eta = 3$. The temporal emission pattern has been time averaged for about a millisecond (duration of sprite). The column-integrated emission intensity was about 100 kR for an optimal optical path.

peak emission intensity for an optimal column integration is about 100 kR.

The emission intensity depends on the type of discharge. The maximum intensity in kilorayleighs for a optimal column integration along the x axis is shown in Figure 9 as a function of the dimension of the discharge $D(\eta)$. Since the optical emission intensity is extremely sensitive to the power density, a factor of 2 on the electric field strength can have profound effects on the emission pattern of a given fractal discharge.

As seen in Figure 9, different fractals require different current peaks (or propagation speed) to produce similar emissions intensities. For the four fractals of Figure 7 we find the necessary current peak I_o needed to produce an emission intensity of about 100 kR. The corresponding emission patterns are shown in Figure 10 with their peak current I_o, which is related to the total charge discharge as seen above. We note that the emission pattern corresponding to the fractal $\eta = 3$ has considerable spatial structure as compared with the other cases in the figure. We see that by having a spatially structured radiation pattern, the fractals can increase the power density

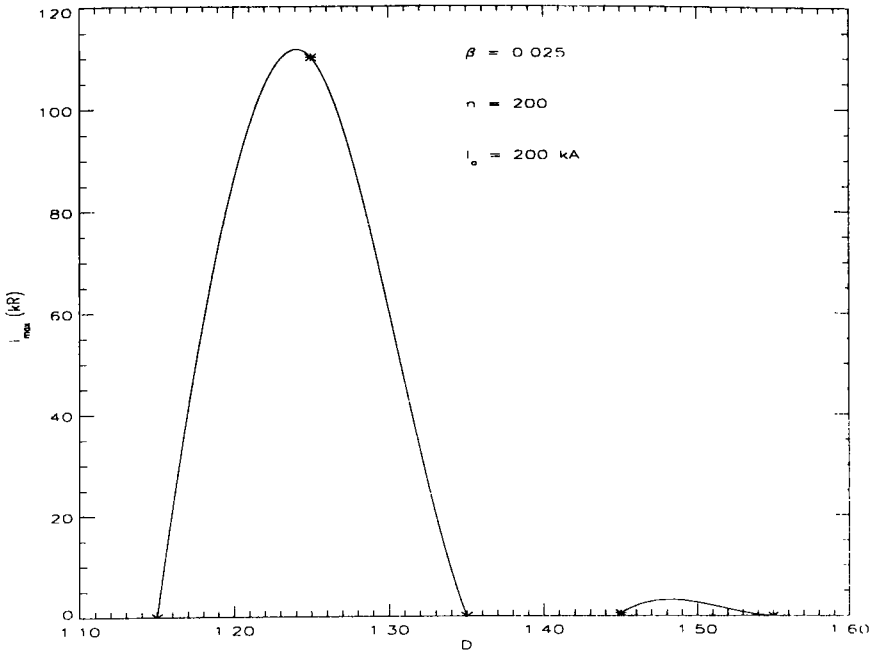

Figure 9. The maximum intensity in kilorayleighs as a function of the dimension. The graph has been interpolated by a cubic spline, but the actual points are shown by asterisks.

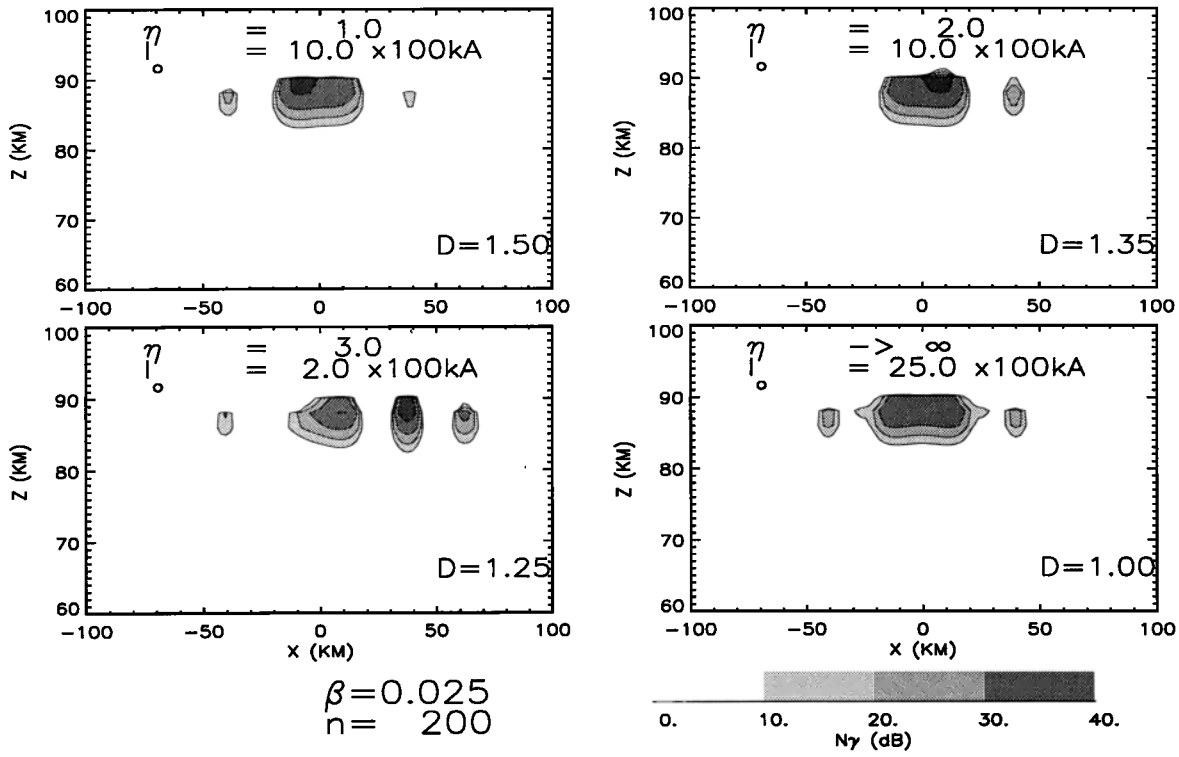

Figure 10. The emissions patterns at the line y =10 km corresponding to the four fractal structures of Figure 7 which have dimensions $D \simeq 1.5$, 1.35, 1.25, and 1.0. The current is chosen so that the peak emission intensity is about I(kR)$\simeq$100 kR, and $\beta = 0.025$.

locally in specific regions of the ionosphere and generate considerable optical emissions with relatively low (more realistic) lightning discharge parameters.

5. Conclusions and Discussions

A novel model (Figure 1) for the formation of red sprites, which incorporates the fractal nature of the horizontal lightning discharges or of a spider lightning type, was presented. The fractal structure of the discharge is reflected in the subsequent optical emission pattern. Such a model fits the qualitative model for the generation of red sprites by *Lyons* [1996], which is based on the fact that horizontal discharges of the order of 100 km have been observed in connection with positive cloud-to-groud (+CG) events. The model starts with the initial spider lightning followed by the positive leader toward the ground, which, in turn, is followed by the positive return stroke. The latter acts as a charge put in the center of a Lichtenberg-like figure, i.e., the lightning discharge propagates along the spider channel. Evidence for these types of models has been obtained from a set of measurements of the properties of the discharges in correlation with the sprites. Red sprites seem to be uniquely correlated with +CG discharges, but only some of the +CG discharges actually generate sprites. Time correlation studies of the time delay between the +CG events and the associated sprite have shown that it can reach more than tens, and sometimes hundreds, of milliseconds [*Lyons*, 1996], suggestive of the time delay required to develop the horizontal intracloud fractal discharge. As mentioned by *Lyons* [1996] the sprite-generating storms seem to have dimensions in excess of 100 km. Such large sizes are also required for the generation of the long horizontal discharges. The similarity between lightning discharges and dielectric breakdown helps to understand the role played by +CG discharges in red sprite generation. Surface dielectric breakdown develops a much more intense structure if caused by an immerse positive needle rather than

by a negative one, as revealed by the Lichtenberg figures given by *Atten and Saker* [1993]. A simple physical explanation of this effect is that the positively charged needle pulls electrons from the media, which is more energetically efficient than pushing electrons ejected by the negatively charged needle. Similarly, the intracloud lightning discharge will acquire a better developed fractal structure if caused by a positive rather than a negative return stroke.

For an optimal configuration, so that the fields get projected upward, the lightning discharge must be horizontal, i.e., the so-called intracloud lightning or "spider lightning" [*Lyons*, 1994]. According to *Lyons* [1996], lightning discharges having a peak current of up to 200 kA are associated with sprites. We assume that a fraction of this current will be deflected from the cloud back into the lightning channel, while approximately half of the peak current will go to the intracloud discharge. Thus the intracloud current peak could reach almost 100 kA. Statistics of the speed of propagation for intracloud lightning are incomplete. The propagation speed during a cloud-to-ground return stroke can reach speeds of about $\beta \approx 0.1$-0.5 [*Uman*, 1987], while the propagation speed of intracloud discharges is at least an order of magnitude lower, and hence we take $\beta \approx 0.01$-0.05.

Certain fractals can radiate more effectively than others, but, in general, this problem is very complicated. The power density, and thus the emission pattern and intensity, scales as $S(W/m^2) \approx \beta^2 I_o^2 \ f(D)g(\theta)$ in the far field of the small line elements. For a specific dimension, i.e., $D(\eta = 3) \simeq 1.25$, we obtained an emission intensity of about 100 kR, with $\beta = 0.025$ and $I_o = 200$ kA. However, using the above scaling for the radiated field, we can generate a similar radiation pattern with $\beta = 0.05$ and $I_o = 100$ kA. The optical emission pattern depends on the structure of the discharge, but we conjecture that the most relevant structural parameter in determining the spatial structure of the emissions is the dimension of the self-similar fractal. Even though we live in a world where dielectric discharges seem to have $D \approx 1.6$ [*Sander*, 1986; *Niemeyer et al.*, 1984], lightning discharges seem to show lower dimensions, a fact that might become relevant due to the sensitivity of the emission strength on the fractal dimension of the discharge. The optimal emissions intensity is obtained for dimensions $D \simeq 1.25$ for the fractal model used above. In this case, the ionization starts occurring for $I_o > 200$ kA and $\beta = 0.025$ (i.e., for $I_o > 200$ kA the equation for the evolution of the electron density n_e should be included).

It can be observed from our model of sprites that the main body of the sprites is constrained between 80 and 90 km in height. The latest observations of sprites reveal filaments that can be described as streamers [*Cummer and Inan*, 1997] propagating down from the main body of the sprite with a cross-sectional diameter of 100 m or less. Given the nucleated spatial structure in the conductivity produced by the fractal lightning discharge, the streamers would start naturally in the presence of a laminar field. The laminar field includes the field induced in the ionosphere during the cloud charging process. Also, some effect might come from the near-zone field described in equation (14). Therefore a comprehensive model of sprites, which includes the main body produced by the fractal lightning and the subsequent streamer development, has to be developed. It involves both the laminar and electromagnetic lightning-induced fields and their effects in the lower ionosphere can be developed from a model that solves the nonlinear wave equation, equation (7), and includes ionization and charge separation. Such streamer concept naturally allows for the expansion of the heated region (of the sprite) to a wider range in heights.

Appendix: Electric Fields From the Fractal

A current pulse propagates with speed $\beta = \mathrm{v/c}$ along a fractal structure. At the nth line element with orientation $\mathbf{L_n}$ and length L_n, which is parametrized by $l \in [0, L_n]$, the current is given by $J_n(s_n, l, t) = I_n \ I(t - s_n + l/\mathrm{v})$ (the time dependence $I(t)$ is given by equation 4), where s_n is the path length along the fractal (or if you prefer, a phase shift). The radiation field is the superposition, with the respective phases, of the small line current elements that form the fractal. For a set $\{\mathbf{r_n}, \mathbf{L_n}, \mathbf{I_n}, \mathbf{s_n} \,|\, \mathbf{n} = \mathbf{0}, ..., \mathbf{N}\}$ of line elements, the Fourier transformed hertz vector is given by

$$\mathbf{\Pi}(\mathbf{x}, \omega) = \sum_{\{\mathbf{n}\}} \frac{\mathbf{i}\widehat{\mathbf{L}}_\mathbf{n}}{\omega} \int_0^{\mathbf{L_n}} \frac{\mathbf{J_n}(\mathbf{s_n}, \mathbf{l}, \omega)\, \mathbf{e}^{\mathbf{ik}\|\mathbf{x}-\mathbf{r_n}-\mathbf{l}\widehat{\mathbf{L}}_\mathbf{n}\|}}{\| \mathbf{x} - \mathbf{r_n} - \mathbf{l}\widehat{\mathbf{L}}_\mathbf{n} \|} \mathbf{dl}, \tag{13}$$

as a solution to Maxwell's equations. Here I_n is the strength of the current at the nth line element, s_n is the path length along the fractal, r_n is the position

of the element, $J_n(s_n, l, \omega) = I_n\, I(\omega) e^{i\frac{\omega}{v}(s_n+l)}$ is the Fourier-transformed current strength at the nth line element, $\mathbf{x}$ is the position at which we measure the fields, ω is the frequency, and $k = \frac{\omega}{c}$. Values with the circumflex indicate unit vectors, and $d_n = \| \mathbf{x} - \mathbf{r_n} \|$ means the standard distance from the line element to the field position.

To simplify the notation, we will denote $\mathbf{d_n} = \mathbf{x} - \mathbf{r_n}$. Note that, in general, the size of a single element $L_n \approx 100$ m is much smaller than the distance to the ionosphere $d_n \approx 80$ km, i.e., $L_n \ll d_n$. Therefore we can use the far-field approximation of the small elements to carry the above integral. Of course, the nonuniformity in the radiation pattern will be due to the phase coherence, or interference pattern, between the different elements that form the fractal. The electric field is then constructed from $\mathbf{E}(\mathbf{x}, \omega) = \nabla \times \nabla \times \mathbf{\Pi}(\mathbf{x}, \omega)$. We then invert the Fourier transform of the field to real time and obtain the spatiotemporal radiation pattern due to the fractal discharge structure, which is given by

$$\mathbf{E}(\mathbf{x}, \mathbf{t}) = \sum_{\{\mathbf{n}\}} \frac{\beta \mathbf{I_n}}{\mathbf{c d_n}(1 - \beta(\hat{\mathbf{L}}_\mathbf{n} \cdot \hat{\mathbf{d}}_\mathbf{n}))}$$

$$\{\hat{\mathbf{L}}_n \left[I + \frac{c}{d_n} I_1 + \frac{c^2}{d_n^2} I_2 \right]_{t-\tau_2}^{t-\tau_1}$$

$$-\hat{\mathbf{d}}_n (\hat{\mathbf{L}}_n \cdot \hat{\mathbf{d}}_n) \left[I + \frac{3c}{d_n} I_1 + \frac{3c^2}{d_n^2} I_2 \right]_{t-\tau_2}^{t-\tau_1} \} \qquad (14)$$

where

$$I_1(t) = \int_{-\infty}^{t} d\tau I(\tau)$$

$$I_2(t) = \int_{-\infty}^{t} d\tau \int_{-\infty}^{\tau} d\tau' I(\tau')$$

can be calculated exactly for the current described above and where

$$\tau_1 = \frac{d_n}{c} + \frac{s_n}{\mathrm{v}}$$

$$\tau_2 = \frac{d_n + (\hat{\mathbf{L}}_n \cdot \hat{\mathbf{d}}_n) L_n}{c} + \frac{s_n + L_n}{\mathrm{v}}$$

The values of τ_1 and τ_2 correspond to the causal time delays from the two endpoints of the line element.

For simplicity we will compute the electric field in the far-field approximation of equation (14) for the small line elements ($kd_n < 2\pi$), and this is given by

$$\mathbf{E}(\mathbf{x}, \mathbf{t}) = \sum_{\{\mathbf{n}\}} \frac{\beta \mathbf{I_n}\, \mathbf{I}(\tau) \,|_{\mathbf{t}-\tau_2}^{\mathbf{t}-\tau_1}}{\mathbf{c d_n}(1 - \beta(\hat{\mathbf{L}}_\mathbf{n} \cdot \hat{\mathbf{d}}_\mathbf{n}))} \hat{\mathbf{L}}_\mathbf{n} \qquad (15)$$

Acknowledgments. The work was supported by NSF grant ATM 9422594. We express our gratitude to A. V. Gurevich, A. S. Sharma, and V. A. Rakov for enlightening discussions. We also thank one of the referees, who gave us very helpful comments.

References

Atten, P., and A. Saker, Streamer propagation over a liquid/solid interface, *IEEE Trans. Electr. Insul. 28*, 230, 1993.

Allain, C., and M. Cloitre, Spatial spectrum of a general family of self-similar arrays, *Phys. Rev. A, 36*, 5751-5757, 1987.

Boeck, W. L., O. H. Vaughan Jr., R. Blakeslee, B. Vonnegut B. and Brook M., Lightning induced brightening in the airglow layer, *Geophys. Res. Lett., 19*, 99-102, 1992.

Cummer, S. A., and U. S. Inan, Measurement of charge transfer in sprite-producing lightning using ELF radio atmospherics, *Geophys. Res. Lett., 24*, 1731-1734, 1997.

Femia, N., L. Niemeyer and V. Tucci, Fractal characteristics of electrical discharges: Experiments and simulations, *J. Phys D. Appl. Phys., 26*, 619-627, 1993.

Franz, R. C., R. J. Memzek R., and J. R. Winckler, Television image of a large upward electrical discharge above a thunderstorm system, *Science, 249*, 48-51, 1990.

Goodman, J. W., *Statistical Optics*, Wiley-Intersci., New York, 1985.

Gurevich, A. V., *Nonlinear Phenomena in the Ionosphere*, Springer-Verlag, New York, 1978.

Idone, V. P., Microscale tortuosity and its variation as observed in triggered lightning channels, *J. Geophys. Res.,100*, 22,943-22,956, 1995.

Jaggard D. L., On fractal electrodynamics, in *Recent Advances in Electromagnetic Theory*, edited by H. N. Kritikos and D. L. Jaggard, Springer-Verlag, New York, 1990.

Kerr, R. A., Atmospheric scientists puzzle over high altitude flashes, *Science, 264*, 1250-1251, 1994.

Kim, Y., and D. L. Jaggard, The fractal random array, *Proc. IEEE, 74*(9), 1278-1280, 1986.

Lyons, W. A., Characteristics of luminous structures in the stratosphere above thunderstorms as imaged

by low-light video, *Geophys. Res. Lett., 21*, 875-878, 1994.

Lyons, W. A., Sprite observations above the U.S. High Plains in relation to their parent thunderstorm systems, *J. Geophys. Res, 101*, 29,641-29,652, 1996.

Le Vine, D. M., and R. Meneghini, Simulation of radiation from lightning return strokes: The effects of tortuosity, *Radio Sci., 13*, 801-809, 1978.

Mende, S. B., R. L. Rairden, G. R. Swenson, and W. A. Lyons, Sprite Spectra; N2 1 PG band identification, *Geophys. Res. Lett., 22*, 2633-2636, 1995.

Milikh, G. M., K. Papadopoulos, and C. L. Chang, On the physics of high altitude lightning, *Geophys. Res. Lett., 22*, 85-88, 1995.

Milikh G. M., J. A. Valdivia, and K. Papadopoulos, Model of red sprite optical spectra, *Geophys. Res. Lett., 24*, 833-836, 1997.

Niemeyer, L., L. Pietronero, and H. J. Wiesmann, Fractal dimension of dielectric breakdown, *Phys. Rev. Lett., 52*, 1033-1036, 1984.

Ott, E., *Chaos in Dynamical Systems*, Cambridge Univ. Press, New York, 1993.

Papadopoulos, K., G. Milikh, A. V. Gurevich, A. Drobot, and R. Shanny, Ionization rates for atmospheric and ionospheric breakdown, *J. Geophys. Res., 98*, 17,593-17,596, 1993.

Pasko, V. P., U. S. Inan, Y. N. Taranenko, and T. Bell, Heating, ionization and upward discharges in the mesosphere due to intense quasi-electrostatic thundercloud fields, *Geophys. Res. Lett.*, **22**, 365-368, 1995.

Rowland, H. L., R. F. Fernsler, J. D. Huba, and P. A. Bernhardt, Lightning driven EMP in the upper atmosphere, *Geophys. Res. Lett., 22*, 361-364, 1995.

Sander, L. M., Fractal growth process, *Nature, 322*, 789-793, 1986.

Sentman, D. D. and E. M. Wescott, Observations of upper atmospheric optical flashes recorded from an aircraft, *Geophys. Res. Lett., 20*, 2857-2860, 1993.

Sentman, D. D., E. M. Wescott, D. L. Osborne, D. L. Hampton, and M. J. Heavner, Preliminary results from the Sprites94 aircraft campaign, 1, Red sprites, *Geophys. Res. Lett, 22*, 1205-1208, 1995.

Tsang, K., K. Papadopoulos, A. Drobot, P. Vitello, T. Wallace, and R. Shanny, RF ionization of the lower ionosphere, *Radio Sci., 20*, 1345-1360, 1991.

Uman, M. A., *The Lightning Discharge*, Academic, San Diego, Calif., 1987.

Vaughan, O. H. Jr., R. Blakeslee, W. L. Boeck, B. Vonnegut, M. Brook, and J. McKune Jr., A cloud-to-space lightning as recorded by the Space Shuttle payload-bay TV cameras, *Mon. Weather Rev., 120* , 1459-1461, 1992.

Valdivia, J. A., G. Milikh, and K. Papadopoulos, Red sprites: lightning as a fractal antenna, *Geophys. Res. Lett., 24*, 3169-3172, 1997.

Vecchi, G., D. Labate, and F. Canavero, Fractal approach to lightning radiation on a tortuous channel, *Radio Sci., 29*, 691-704, 1994.

Werner, D. H., and P. L. Werner, On the synthesis of fractal radiation patterns, *Radio Sci., 30*, 29-45, 1995.

Williams, E. R., The electrification of thunderstorms, *Sci. Am.*, 88-89, November, 1988.

Winckler, J. R., R. C. Franz, and R. J. Nemzek, Fast low-level light pulses from the night sky observed with the SKYFLASH program, *J. Geophys. Res., 98*, 8775-8783, 1993.

Winckler, J. R., W. A. Lyons, T. E. Nelson, and R. J. Nemzek, New high-resolution ground-based studies of sprites, *J. Geophys. Res. 101*, 6997-7004, 1996.

G. .M Milikh, Department of Astronomy, University of Maryland, College Park, MD 20742.

K. Papadopoulos, Department of Physics, University of Maryland, College Park, MD 20742.

J. A. Valdivia, NRC NASA Goddard Space Flight Center, Code 692, Greenbelt, MD 20771. (e-mail: alejo@roselott.gsfc.nasa.gov)

(Received June 5, 1997; revised June 11, 1998; accepted June 30, 1998.)